Scaling Distributed Optimal Renewable Energy Coordination in Unbalanced Distribution Systems

Rabayet Sadnan *Member, IEEE*, Nathan Gray *Student Member, IEEE*, Anjan Bose, *Fellow, IEEE*, Anamika Dubey, *Senior Member, IEEE*, and Kevin P. Schneider, *Fellow, IEEE*

***Abstract*—The increased installation of renewable grid-edge assets into an already complex power distribution system has driven extensive development of distributed optimal power flow (OPF) methods to coordinate such assets. However, existing distributed optimization algorithms applied to unbalanced systems require many communication rounds among the distributed agents and may pose convergence challenges. Besides, the communication network parameters also significantly impact the algorithm's performance. In this paper, we propose a scalable, equivalent network approximation-based, distributed OPF method that employs a communication infrastructure using cyber-physical co-simulation platform to coordinate grid-edge renewable assets for three-phase unbalanced distribution systems. Additionally, the robustness of the proposed approach is validated under stressed communication scenarios. The results are thoroughly compared with the state-of-the-art algorithms and equivalent centralized optimal power flow (C-OPF) problems for medium IEEE-123 bus test system and large-scale PNNL R3-12.47-2 feeder distribution test systems.**

***Index Terms*—Distributed OPF, unbalanced distribution system, distributed energy resources, renewable energy coordination, co-simulation.**

I. Introduction

To efficiently coordinate the growing numbers of grid-edge assets, such as distributed energy resources (DERs) and photovoltaics (PVs), optimal power flow (OPF) problems for power distribution systems have gained significant attention recently [1], [2]. Traditionally, the distribution system is centrally managed to coordinate DERs and other grid-edge technologies. With the increasing number of such controllable assets and growing system complexity, such a system suffers from several challenges including poor scalability, and susceptibility to single-point failures [3], [4]. The additional complexities introduced by the three-phase, unbalanced power distribution systems may pose convergence issues for the centralized optimization problems and may result in failure to attain the optimal solution within a reasonable time [4]. Besides, a centrally managed system is impractical for emerging distribution systems typically composed of several geographically separated areas controlled by different entities that may not want to share models and/or data. Thus, as modern distribution grids evolve, decentralized data and distributed control architecture are becoming essential [5].

The existing literature has shown the applicability of the distributed optimization paradigm in reducing the computational requirements for OPF problems and in mitigating other challenges including ownership boundaries and avoiding single-point failures [4], [6]. To this end, general distributed optimization techniques, such as, alternating direction method of multipliers (ADMM), Auxiliary Problem Principle (APP), etc. have been adopted to solve distributed OPF (D-OPF) problems for power distribution systems [6]–[11]. Generally, D-OPF algorithms involve two iterative processes: (i) sub-problem optimization involving *micro-iterations*, where distributed agents individually solve optimization problems specific to their areas; the nature of the optimization problems, such as nonlinear vs. convex, etc., dictates the number of micro-iterations needed. And (ii) distributed coordination requiring *macro-iterations*, where distributed agents exchange the boundary variables with their neighbors; also referred to as communication-rounds. The overall compute complexity of the algorithm depends on the total number of micro- and macro-iterations required to achieve network-level convergence. Traditional algorithms suffer from the convergence issues at the boundaries, experiencing slow or no convergence for the macro-iteration steps [4], [8], [12]. This calls for algorithmic advances in D-OPF algorithms to realistically apply them to the real-world power distribution systems.

Furthermore, traditional D-OPF methods either neglect the impact of communication networks, limiting their practical use, or are too slow for effective implementation. These methods necessitate an expensive communication infrastructure characterized by high bandwidth and low communication delays. This is attributed to the requirements of substantial number of macro-iterations to converge for relatively small and/or balanced systems [4], [6], [8], [13], [14]. Although real-time feedback-based online distributed algorithms address some of the challenges [12], [15]–[17], they still require thousands of time-steps to track the optimal solution, resulting in a sub-optimal system operation and constraint violations. Recently, authors proposed an algorithm based on the structure of the power flow problem for a balanced radial distribution system that drastically reduces the number of macro-iterations [18]. However, the performance of the D-OPF algorithm has not been evaluated in a realistic cyber-physical environment with appropriate models for communication systems for scaled unbalanced distribution systems with detailed system models.

Thus, the objective of this paper is to develop a fast, computationally tractable, and communication-efficient offline D-OPF algorithm for coordinating grid-edge assets in unbalanced active power distribution systems, incorporating comprehensive system models to represent realistic network conditions. The developed method aligns with the distributed control architecture essential for modern, evolving power distribution systems. The unbalanced nature of the system increases OPF

Rabayet Sadnan and Kevin P. Schneider are with Pacific Northwest National Laboratory (PNNL), USA, and Nathan Gray, Anjan Bose and Anamika Dubey are with the Department of EECS, WSU, Pullman, WA-99164, USA; e-mail: rabayet.sadnan@pnnl.gov. This work is supported in part by the NSF Career Award under Grant 1944142 and in part by the U.S. Department of Energy under Grant DE-AC05-76RL01830.

challenges due to the scale of the problem and added power flow model complexities, stemming from the mutual coupling in the unbalanced network. Our approach leverages the radial operation of distribution systems in North America [19] and employs a distributed coordination algorithm to achieve a computationally efficient and near-optimal D-OPF solution that requires low fidelity communication infrastructure properties. Additionally, we have implemented the algorithm in a realistic communication network to emphasize the critical role of communication in distributed OPF methods. This implementation, previously lacking in literature, highlights the method's practical viability. Specifically, our contributions are:

- Development of a decomposition-based D-OPF method for 3-phase unbalanced distribution system
- Demonstration of scalability of the proposed method using larger 3-phase unbalanced system, showcasing the relevance of complex and real-world distribution networks.
- Integration of a communication network through co-simulation to demonstrate the feasibility with realistic constraints.
- Through comparison with state-of-the-art offline ADMM-based D-OPF and online feedback-based D-OPF method.
- Demonstration of the effectiveness of our proposed method when faced with increased complexity, including the addition of controllable legacy devices that adds nonlinearity (integer variables) in the OPF problem.

II. Network Modeling & Problem Formulation

In this paper, $(\cdot)^T$ represents matrix transpose; $(\cdot)^*$ represents the complex-conjugate; $\overline{(\cdot)}$ & $\underline{(\cdot)}$ denotes the max and min of a variable; $(\cdot)^{(n)}$ represents the n^{th} iteration; $\mathbb{R}, \mathbb{I}$ denotes the real, imaginary part of the complex number, respectively; the superscript p (without parenthesis) denotes the three-phases, i.e., $\{a, b, c\}$ of the system.

A. Power Flow Model

This section details the power flow models to formulate the OPF problems for an unbalanced power distribution system. The unbalanced power flow equations are based on our prior work [20]. Let us consider an unbalanced radial power distribution network of n buses where, $\mathcal{N}$ denotes the set of buses in that system and $\mathcal{E}$ denotes the set of edges identifying distribution lines that connect the ordered pair of buses $\{ij\}$, $\forall\ i, j \in \mathcal{N}$. Here, ϕ_j denotes the set of phases in the bus j. Let $v_j^p = |V_j^p|^2$ be the squared magnitude of voltage at bus $j \in \mathcal{N}$ for phase $p \in \phi_j$. Define $\phi_{ij} = \{pq : p \in \phi_i \text{ and } q \in \phi_j\ \forall \{ij\} \in \mathcal{E}\}$. Let $l_{ij}^{pq} = (|I_{ij}^{pp}||I_{ij}^{qq}|)$ be the squared magnitude of the line current flowing in the phase $pq \in \phi_{ij}$ of line (i, j); i.e., the term l_{ij}^{pq} is a mathematical abstraction representing the product of the magnitudes of branch currents in phases p and q. Also, $S_{ij}^{pq} = P_{ij}^{pq} + jQ_{ij}^{pq}$ and $z_{ij}^{pq} = r_{ij}^{pq} + jx_{ij}^{pq}$, where $pq \in \phi_{ij}$. Variable $p_{L,j}^p$ and $q_{L,j}^p$ denote the active and reactive load (respectively) connected at node j of phase $p \in \phi_j$. Similarly, subscript D, j denotes the DER generation at node j; e.g., $p_{D,j}^p$ denotes the active power generation at node j for phase p. δ_{ij}^{pq} is the angle difference between the phase currents. First, we define the nonlinear power flow model and then the linearized model is detailed.

1) Nonlinear Model: With the approximated phase voltage and branch current angles, [20] developed the nonlinear power flow model for an unbalanced radial power distribution system. The model is defined below in (1). The loads can be modeled as voltage dependent loads as formulated in the Appendix.

$$P_{ij}^{pp} - \sum_{q\in\phi_j} l_{ij}^{pq}\left(r_{ij}^{pq}\cos(\delta_{ij}^{pq}) - x_{ij}^{pq}\sin(\delta_{ij}^{pq})\right) = \sum_{k:j\to k} P_{jk}^{pp} + p_{L,j}^p - p_{D,j}^p \tag{1a}$$

$$Q_{ij}^{pp} - \sum_{q\in\phi_j} l_{ij}^{pq}\left(x_{ij}^{pq}\cos(\delta_{ij}^{pq}) + r_{ij}^{pq}\sin(\delta_{ij}^{pq})\right) = \sum_{k:j\to k} Q_{jk}^{pp} + q_{L,j}^p - q_{D,j}^p - q_{C,j}^p \tag{1b}$$

$$v_j^p = v_i^p - \sum_{q\in\phi_j} 2\mathbb{R}\left[S_{ij}^{pq}(z_{ij}^{pq})^*\right] + \sum_{q\in\phi_j} z_{ij}^{pq} l_{ij}^{qq} + \sum_{q1,q2\in\phi_j, q1\neq q2} 2\mathbb{R}\left[z_{ij}^{pq1} l_{ij}^{q1q2}\left(\angle(\delta_{ij}^{q1q2})\right)(z_{ij}^{pq2})^*\right] \tag{1c}$$

$$(P_{ij}^{pp})^2 + (Q_{ij}^{pp})^2 = v_i^p l_{ij}^{pp} \tag{1d}$$

$$(l_{ij}^{pq})^2 = l_{ij}^{pp} l_{ij}^{qq} \tag{1e}$$

2) Linear-approximated Model: The computational complexity augmented by the nonlinear power flow models to the existing scalability issues associated with large-scale OPF problems can be reduced using the approximated linearized power flow models. In equation (2), a linear-approximated power flow model – known as the three-phase LinDistFlow model is defined. The assumption is that the line loses are negligible compared to the power flow in the system; however, line impedances are included in the formulation to compute the voltage drops across the lines. [20], [21].

$$P_{ij}^{pp} = \sum_{k:j\to k} P_{jk}^{pp} + p_{L,j}^p - p_{D,j}^p \tag{2a}$$

$$Q_{ij}^{pp} = \sum_{k:j\to k} Q_{jk}^{pp} + q_{L,j}^p - q_{D,j}^p - q_{C,j}^p \tag{2b}$$

$$v_j^p = v_i^p - \sum_{q\in\phi_j} 2\mathbb{R}\left[S_{ij}^{pq}(z_{ij}^{pq})^*\right] \tag{2c}$$

B. DER Modeling

We define a general DER model for different network objectives in equation (3)-(5). This DERs are designed as a general model, and can accommodate any renewable energy resources, such as rooftop PVs; thus in this paper, DER and PV models are used interchangeably. The general DER model is defined by equation (3) at node j for phase $p \in \phi_j$. If $S_{DR,j}^p$ is defined as the nominal rating of the DER at node j for phase $p \in \phi_j$, then the reactive power generation ($q_{D,j}^p$) and the active power generation ($p_{D,j}^p$) of the DER are constrained by the nominal rating of the DER. When $q_{D,j}^p$ is modeled as the decision variable, $p_{D,j}^p$ is assumed to measured and known. For this case, the DER model evolves from a quadratic inequality (3) to a linear inequality (4) constraint. On the contrary, when the active power generation, $p_{D,j}^p$ is set as decision variables, we assume $q_{D,j}^p = 0$, and the DER model is defined by the linear inequality (5). However, for both real and reactive power

control, DERs can be linearly approximated, as shown in the Appendix.

$$\left(p^p_{D,j}\right)^2 + \left(q^p_{D,j}\right)^2 \leq \left(S^p_{DR,j}\right)^2 \tag{3}$$

$$-\sqrt{(S^p_{DR,j})^2 - (p^p_{D,j})^2} \leq q^p_{D,j} \leq \sqrt{(S^p_{DR,j})^2 - (p^p_{D,j})^2} \tag{4}$$

$$0 \leq p^p_{D,j} \leq S^p_{DR,j} \tag{5}$$

C. Centralized OPF (C-OPF) Problem

In this section, we define the C-OPF problems for an unbalanced radial distribution system, that can be solved using a central controller; both nonlinear and linear power flow models have been used for such OPF problems for the unbalanced distribution system.

1) Loss Minimization: First, the active power loss minimization problem has been formulated where the line loss is reduced by generating optimal $q^p_{D,j}$, without violating operational limits. The optimization variable is $X = [P^{pp}_{ij}, Q^{pp}_{ij}, v^p_j, l^{pq}_{ij}, q^p_{D,j}]^T$, $\forall j \in \mathcal{N}$ & $\forall \{ij\} \in \mathcal{E}$. The OPF problem **(C1)** is defined in (6) using nonlinear power flow models. Here, $\left(I^{rated}_{ij}\right)^2$ is the thermal limit for the line $\{ij\} \in \mathcal{E}$, and $\overline{v}$ & $\underline{v}$ denote the limits on the squared magnitude of the nodal voltages.

$$\textbf{(C1)} \quad \min \sum_{p\in\phi_j, j:i\to j} l^{pp}_{ij} r^{pp}_{ij} \tag{6a}$$

$$\text{s.t.} \quad \text{equation (1) \& (4)} \tag{6b}$$

$$l^p_{ij} \leq \left(I^{rated}_{ij}\right)^2 \ \& \quad \underline{v} \leq v^p_j \leq \overline{v} \tag{6c}$$

By substituting the nonlinear power flow model with the linear approximated model, a tractable convex C-OPF model for the equivalent optimization problem can be devised (Problem **(C2)** in (7)). Additionally, all the nodal voltages are assumed as 1.00 p.u. to approximate the objective function (active power line loss) by a convex cost function: $\sum \left(\left(P^{pp}_{ij}\right)^2 + \left(Q^{pp}_{ij}\right)^2 \right) r^{pp}_{ij}$ for all edges $\{ij\} \in \mathcal{E}$. Here the optimization variable is $X = [P^{pp}_{ij}, Q^{pp}_{ij}, v^p_j, q^p_{D,j}]^T$, $\forall j \in \mathcal{N}$ & $\forall \{ij\} \in \mathcal{E}$.

$$\textbf{(C2)} \quad \min \sum_{p\in\phi_j, j:i\to j} \left(\left(P^{pp}_{ij}\right)^2 + \left(Q^{pp}_{ij}\right)^2 \right) r^{pp}_{ij} \tag{7a}$$

$$\text{s.t.} \quad \text{equation (2) \& (4)} \tag{7b}$$

$$\underline{v} \leq v^p_j \leq \overline{v} \tag{7c}$$

2) DER Curtailment Minimization: In the DER curtailment minimization problem, active power generations from the DERs are expressed as control variables. Specifically, the network objective is to maximize active power generations from each individual DERs, or equivalently, minimize the power curtailments from all the DERs in all of the phases, without exceeding any operational limits. For the DER curtailment minimization OPF, the optimization variable is $X = [P^{pp}_{ij}, Q^{pp}_{ij}, v^p_j, l^{pq}_{ij}, p^p_{D,j}]^T$, $\forall j \in \mathcal{N}$ & $\forall \{ij\} \in \mathcal{E}$. The OPF problem **(C3)** is defined in (8) using the nonlinear power flow models. Here, $\overline{p^p_{D,j}}$ denotes the maximum available power generation at node j for phase p

$$\textbf{(C3)} \quad \min \sum_{\forall j\in\mathcal{N}} \sum_{p\in\phi_j} (\overline{p^p_{D,j}} - p^p_{D,j})^2 \tag{8a}$$

$$\text{s.t.} \quad \text{equation (1) \& (5)} \tag{8b}$$

$$l^p_{ij} \leq \left(I^{rated}_{ij}\right)^2 \ \& \quad \underline{v} \leq v^p_j \leq \overline{v} \tag{8c}$$

Further, the DER curtailment minimization problem can be formulated as a convex OPF problem with linear-approximated power flow model (eqn. (2)). The optimization problem is detailed in (9) and referred as problem **(C4)**. The optimization variable for **(C4)** is $X = [P^{pp}_{ij}, Q^{pp}_{ij}, v^p_j, p^p_{D,j}]^T$, $\forall j \in \mathcal{N}$ & $\forall \{ij\} \in \mathcal{E}$.

$$\textbf{(C4)} \quad \min \sum_{\forall j\in\mathcal{N}} \sum_{p\in\phi_j} (\overline{p^p_{D,j}} - p^p_{D,j})^2 \tag{9a}$$

$$\text{s.t.} \quad \text{equation (2) \& (5)} \tag{9b}$$

$$\underline{v} \leq v^p_j \leq \overline{v} \tag{9c}$$

III. Distributed Coordination Algorithm

The optimization problem for radial power distribution networks – composed of several connected areas, are naturally decomposable into multiple sub-problems defined for the areas. In this section, first we detail the decomposition approach for the OPF problems of three-phase unbalanced systems, and then the local sub-problems are defined. The proposed distributed optimization method utilizes the equivalent network approximation (ENApp) model for the radial distribution system. Later, we briefly discuss the developed cyber-physical co-simulation platform, where both the physical and the communication layer are simulated to study the impact of the developed ENApp D-OPF algorithm on a real life distribution network.

A. Decomposition Method & Network Approximations

Let the distribution system be composed of N connected areas, and $\mathcal{A} = \{A_1,\ A_2, \ldots,\ A_N\}$ be the set of all areas. Any Area $A_m \in \mathcal{A}$ is defined as the directed radial graph $A_m = \mathcal{G}(\mathcal{N}_m, \mathcal{E}_m)$; $\mathcal{N}_m$ and $\mathcal{E}_m$ defines the set of nodes and lines in the system. The set of central optimization variables is defined as $X = \bigcup_{m=1}^{N} X_m$, where X_m represents the set of all local optimization variables for Area A_m. Similarly $\mathcal{S} = \bigcup_{m=1}^{N} \mathcal{S}_m$ represent the set of constraints for overall problem, and $\mathcal{S}_m$ represents the local constraints. If central objective $f(X)$ is a decomposable cost function, then the problem can be decomposed into several local sub-problems and written as (10). Here, f_m is defined as the local objective function for Area A_m. The complicating variables, $y_{m'}$ are shared by the neighboring areas of A_m, and are kept constant for solving the local optimization problem in this primal decomposition-based method.

$$\min_{X\in\mathcal{S}} \ f(X) = \sum_{m=1}^{N} \min_{X_m\in\mathcal{S}_m} f_m(X_m, y_{m'}) \tag{10}$$

As the overall system topology was radial to begin with, the decomposed areas of the networks are also connected radially and have unique upstream & downstream sections. This specific structure of the system helps to identify the

This article has been accepted for publication in IEEE Transactions on Sustainable Energy. This is the author's version which has not been fully edited and content may change prior to final publication. Citation information: DOI 10.1109/TSTE.2024.3492976

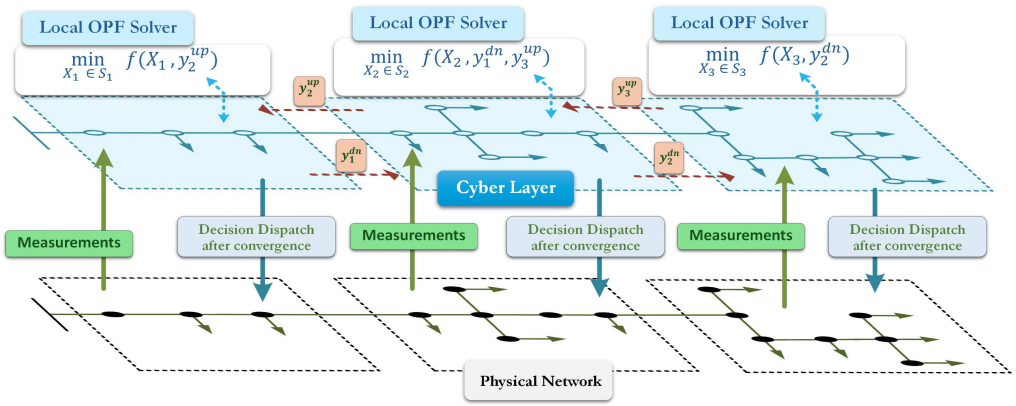

Fig. 1. Pictorial description of the proposed three-phase unbalanced distributed coordination algorithm – ENApp D-OPF.

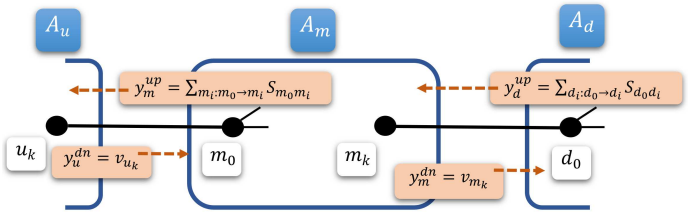

Fig. 2. Network Approximation Model: Each area is sending (i) nodal voltage of the shared bus to the respective downstream area, and (ii) branch power flow incoming from the shared bus with upstream area.

unique parent area and the child areas for any area A_m, which in turns associates the complicating/shared variables, $y_{m'}$ for the local sub-problems – exchanged among the neighboring computing agents to solve the overall problem. For the proposed decomposition approach, the complicating variables are the voltages and the power flows at the shared buses.

First the shared bus is duplicated, and each duplicated bus is assigned for neighboring areas for computing purposes; it is assumed that the duplicated nodes are connected through a low impedance line, which yields negligible voltage drop and power loss in the line. Let for any Area A_m, Area A_u and Area A_d is its parent/Upstream Area (UA) and child/Downstream Area (DA), respectively (Fig. 2). The shared bus between Area A_m and A_u is duplicated and assigned for each area (bus m_0 and bus u_k). Similarly, the shared bus between Area A_m and A_d is duplicated and assigned for each area (bus m_k and bus d_0). Thus the complicating variable for Area A_m is $y_{m'} = [y_u^{dn},\ y_d^{up}]$. In this representation, we have employed the notation where the subscript of shared variable, y, denotes which area computed the variable, while the superscript denotes the variable sharing direction – 'up' means shared with UA, and 'dn' means shared with DA. Specifically, $y_u^{dn} = v_{u_k}$ and $y_d^{up} = \sum_{d_i:d_0 \to d_i} S_{d_o d_i}$; $S_{d_o d_i} = P_{d_o d_i} + jQ_{d_o d_i}$ is the sum of power flows coming out of bus d_0 in Area A_d. For readability purpose, the phase notations are omitted here.

Each area solves related local sub-problems in parallel by assuming the constant complicating variable, i.e., a fixed voltage at the shared bus with the unique UA and constant loads at the shared buses with DAs. Specifically for Area A_m, the voltage at bus m_o is set equal to y_u^{dn}, and the line between bus m_k and bus d_0 is replaced by a constant load with values equal to y_d^{up} at bus m_k. In terms of power system's physics, this approximates the whole upstream and downstream network segments of an Area A_m for radial power distribution systems. After that, the local sub-problem is solved.

After solving local sub-problems, the respective complicating variables, i.e., the total power requirements in the Area A_m ($y_m^{up} = \sum_{m_i:m_0 \to m_i} S_{m_o m_i}$) is shared with UA A_u, and the voltage at bus m_k, i.e., $y_m^{dn} = v_{m_k}$ is shared with DA A_d. Then, the sub-problems are solved again with updated shared variables from the neighbors. When a consensus is attained at all the shared boundaries, then the decision variables are dispatched within the area. The consensus at the boundary can be achieved using Fixed Point Iteration methods (11). The variable Y can be the power flow requirements, y^{up}, or the voltage at the parent node, y^{dn}; (n) denotes the n^{th} iterations. Fig. 1 showcases a pictorial description of the overall D-OPF for a sample 3-Area system.

$$Y^{(n)} := \frac{Y^{(n)} + \alpha Y^{(n-1)}}{1+\alpha} \tag{11}$$

Please note, the proposed decomposition method creates duplicated shared buses between neighbors. However, the decomposition can be done at the sectionalizer switch locations, as those lines also have very low impedances; duplicated shared nodes are not necessary for such decomposition process. Besides, if any area has multiple child/DAs, similar approach can be taken for each DAs. The workflow of the method is described in Algorithm 1.

B. Local Distributed OPF Model

In this section, for Area A_m in Fig. 2, the decomposed local sub-problems at n^{th} macro-iteration, **(D1)-(D4)**, of the corresponding C-OPFs, **(C1)-(C4)** are defined. In the proposed method, each local computing agents solves the corresponding distributed sub-problems, and over macro-iterations, convergence is achieved when all the boundary/shared variables attains consensus.

1) Loss Minimization: The OPF problem **(C1)-(C2)** represent the central formulation of the loss minimization problem using nonlinear and approximated problem, respectively, where the active power line losses are minimized by controlling the reactive power generations from the DERs. We have assumed that the active power is known and controlled by an

This article has been accepted for publication in IEEE Transactions on Sustainable Energy. This is the author's version which has not been fully edited and content may change prior to final publication. Citation information: DOI 10.1109/TSTE.2024.3492976

Algorithm 1: ENApp Distributed OPF for Unbalanced Distribution System

Initialize: Boundary variable values, $Y^{(0)}$; set iteration count n to 0, and ϵ as the tolerance for convergence

Steps :

1 Solve local sub-problem for Area $A_m(\forall A_m \in \mathcal{A})$ in parallel with approximated boundary values.

2 Exchange the solved/calculated boundary variable values for all the phases with the neighboring areas, i.e., send power flow values to the upstream area (UA) and bus voltage magnitude to the downstream areas (DAs).

3 Evaluate the maximum residual at all the boundaries:
$R(n) = max\left(|Y_m^{(n)} - Y_m^{(n-1)}|\right); \forall A_m \in \mathcal{A}.$

4 **If** $R(n) \leq \epsilon$ then consensus is obtained and the optimal decisions are dispatched.

5 **else**, update the boundary variables using equation (11), set iteration count $n = n + 1$ and go to step 1.

MPPT algorithm to maximize the power output. The corresponding decomposed sub-problems for Area A_m, $\forall\{ij\} \in \mathcal{E}_m$ and $\forall j \in \mathcal{N}_m$ are defined in (12)-(13), respectively. Constraint (12c) and (13c) represents the approximated UA and DA with the help of complicating/shared variables, as described in the previous section.

$$\textbf{(D1)} \quad \min \quad f_m(X_m^{(n)}) = \sum_{p\in\phi_j, j:i\to j} l_{ij}^{pp} r_{ij}^{pp} \tag{12a}$$

$$\text{s.t. equation (6b) \& (6c)} \tag{12b}$$

$$v_{m_0}^{p\,(n)} = y_u^{dn,\ p\,(n-1)};$$

$$p_{m_k}^{p\,(n)} = \mathbb{R}[y_d^{up,\ pp\,(n-1)}];\ q_{m_k}^{p\,(n)} = \mathbb{I}[y_d^{up,\ pp\,(n-1)}] \tag{12c}$$

$$\textbf{(D2)} \quad \min \quad f_m(X_m^{(n)}) = \sum_{p\in\phi_j, j:i\to j} \left(\left(P_{ij}^{pp}\right)^2 + \left(Q_{ij}^{pp}\right)^2\right) r_{ij}^{pp} \tag{13a}$$

$$\text{s.t. equation (7b) \& (7c)} \tag{13b}$$

$$v_{m_0}^{p\,(n)} = y_u^{dn,\ p\,(n-1)};$$

$$p_{m_k}^{p\,(n)} = \mathbb{R}[y_d^{up,\ pp\,(n-1)}];\ q_{m_k}^{p\,(n)} = \mathbb{I}[y_d^{up,\ pp\,(n-1)}] \tag{13c}$$

2) DER Curtailment Minimization: The OPF problem **(C3)-(C4)** represent the C-OPF formulation of the DER curtailment minimization problem using nonlinear and approximated models, respectively, where the real power generations for all the phases are maximized within the maximum power point output limits - without violating the operational constraints. Similar to loss minimization objective, the corresponding decomposed sub-problems for Area A_m are defined in (14)-(15), respectively.

$$\textbf{(D3)} \quad \min \quad f_m(X_m^{(n)}) = \sum_{\forall j\in\mathcal{N}_m} \sum_{p\in\phi_j} \left(\overline{p_{D,j}^p} - p_{D,j}^p\right)^2 \tag{14a}$$

$$\text{s.t. equation (8b) \& (8c)} \tag{14b}$$

$$v_{m_0}^{p\,(n)} = y_u^{dn,\ p\,(n-1)};$$

$$p_{m_k}^{p\,(n)} = \mathbb{R}[y_d^{up,\ pp\,(n-1)}];\ q_{m_k}^{p\,(n)} = \mathbb{I}[y_d^{up,\ pp\,(n-1)}] \tag{14c}$$

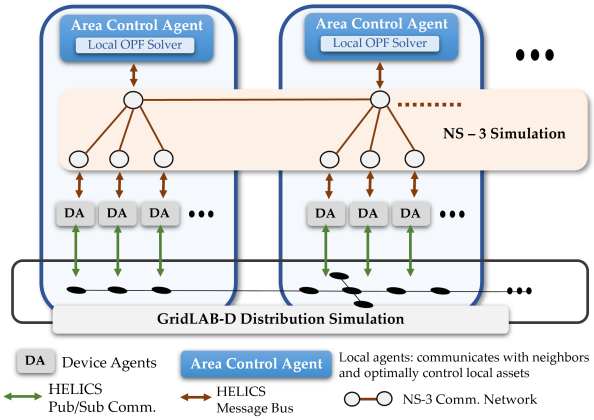

Fig. 3. Co-Simulation structure for Cyber-Physical system

$$\textbf{(D4)} \quad \min \quad f_m(X_m^{(n)}) = \sum_{\forall j\in\mathcal{N}_m} \sum_{p\in\phi_j} \left(\overline{p_{D,j}^p} - p_{D,j}^p\right)^2 \tag{15a}$$

$$\text{s.t. equation (9b) \& (9c)} \tag{15b}$$

$$v_{m_0}^{p\,(n)} = y_u^{dn,\ p\,(n-1)};$$

$$p_{m_k}^{p\,(n)} = \mathbb{R}[y_d^{up,\ pp\,(n-1)}];\ q_{m_k}^{p\,(n)} = \mathbb{I}[y_d^{up,\ pp\,(n-1)}] \tag{15c}$$

C. Co-simulation Platform

A realistic evaluation of distributed algorithms requires modeling the associated communication system. To this end, we developed a multi-agent cyber-physical co-simulation package using HELICS (Hierarchical Engine for Large-scale Infrastructure Co-Simulation), a generic co-simulation platform [22]. Our cyber-physical co-simulation package is composed of the following software: Python 3, GridLAB-D [23], NS-3 [24], which are used to simulate the computing agents, the power distribution networks, the communication networks, respectively. HELICS [22] is then employed to synchronize the simulations and facilitates message passing among the three simulation software (see Fig. 3). Each area has a controller agent shown at the top which has a single connection, via HELICS, to the communication network simulated in NS-3. In this way, the controllers are able to communicate with each other and with the device agents in the local area. The device agents each have a connection, via HELICS, to the physical device simulated in GridLAB-D and to the communication network. The purpose of the device agent is twofold. It formats the raw data it receives from GridLAB-D so the control agent can understand it and it parses commands received from the control agent to the GridLAB-D.

IV. Numerical Simulations

In this section, a detailed evaluation of the proposed ENApp D-OPF algorithm to coordinate grid-edge assets, such as PVs, in three-phase unbalanced distribution systems is presented. First, we have validated our D-OPF approach by comparing the solutions with the equivalent central formulations, and then a comparison is with state-of-the-art ADMM method is detailed. Later, different stressed communication network topologies have been tested to demonstrate the efficacy and robustness of the proposed method. Lastly, a time-series simulation has been performed to showcase the overall usefulness of the proposed method. The simulations were performed on a Core i7-1165G7

TABLE I. Test Systems: Case Parameters

IEEE-123 Bus Test System			
Case	V_{Sub}	**DER Details (per phase)** Rating (kVA)	Active Power (kW)
Loss Min.	1.035	48	20
DER Curt. Min.	1.050	72	60
PNNL R3-12.47-2 Feeder Test System			
Case	V_{Sub}	**Inverter Details (% of load)** Rating	Active Power
Loss Min.	1.035	100%	50%
DER Curt. Min.	1.049	175%	175%

CPU (16 GB RAM) where the approximated problems were solved using *OSQP* solver; the nonlinear OPFs were solved using *fmincon* solver on a Core i7-8550U CPU (16 GB RAM).

A. Simulated System

To test and validate our proposed method, we have run simulations on two different test systems - (i) unbalanced IEEE-123 bus test system, and (ii) unbalanced PNNL R3-12.47-2 feeder [25], each for two optimization objective functions - (i) *loss minimization*, and (ii) *DER curtailment minimization*.

The three-phase unbalanced IEEE-123 bus test system has been modified with 30 three-phase DERs (total of 90 DERs); the test system has overall 261 nodes. The network is split into four distinct control areas (Fig. 4(a)). All DERs in the IEEE-123 bus test system are simulated with uniform apparent power rating and active power output. For the loss minimization objective, DERs have a rating of 48 kVA per phase and an active power output of 20 kW per phase. On the other hand, since the goal of the DER curtailment minimization problem is to produce the maximum amount of active power from each DERs – without violating the voltage constraints, the DER ratings are increased to 72 KVA with a maximum real power output of 60kW per phase (see Table I).

The second system is the larger three-phase unbalanced PNNL R3-12.47-2 feeder, and it has more than 870 nodes in the system. This system has been selected to highlight the convergence of the proposed method for a scaled network. Like the IEEE-123 bus test system, it has been split into 4 distinct control areas (Fig. 4(b)). DERs have been added in proportion to the load on each bus. In the loss minimization objective, DERs have a kVA rating equivalent in value to the kW load on the same bus for each phase. The actual active power generation is set at 50% of the nominal value. In the DER curtailment minimization scenario, the maximum active power generation capacity of the DERs are set to 175% of the rated load at the adjacent node on each phase. For simulations of the PNNL R3-12.47-2 feeder, the substation voltage was set a little lower, at 1.049 for better simulation stability. Unless otherwise specified, all loads were assumed to follow a constant load model.

B. Validation of the Decomposition Method

This section showcases the validation of the proposed distributed OPFs for electric power distribution systems. Specifically, the developed co-simulation platform for distributed OPFs that uses the approximate models, is validated by comparing the resulting objective values for equivalent approximated C-OPF problem and equivalent nonlinear OPF problems (both centralized and distributed). Table II and Table III, show the comparisons between D-OPF and C-OPF results for different cases.

TABLE II. Loss minimization Result Comparison

Method	**Loss (kW)** IEEE-123 Bus System	PNNL R3-12.47-2 Feeder	**Communication-round** IEEE-123 Bus System	PNNL R3-12.47-2 Feeder
Nonlinear Problem				
No OPF	53.338	18.884	-	-
C-OPF	26.305	DNC*	-	-
ENApp D-OPF	26.502	14.2	5	6
Approximated Problem				
C-OPF	26.507	13.646	-	-
ENApp D-OPF	26.546	13.646	5	4
ADMM D-OPF	38.954	DNC*	12	DNC*

1) Optimality: Table II shows the loss minimization case for both test systems for various methods. Both the nonlinear and approximated D-OPF method (ENApp) for unbalanced cases matches the objective values from the equivalent C-OPF objective values. For example, for IEEE-123 bus test system, the nonlinear and approximated ENApp D-OPF solution (line loss) are 26.5 kW and 26.54 kW, which is close to the equivalent nonlinear C-OPF solution (26.3 kW). Please note that, without the optimization, the line loss is 53.338 kW. Moreover, the approximated C-OPF result also matches with the equivalent nonlinear C-OPF solution.

The significance of the proposed method in terms of speed and computational advantages may not be readily apparent for smaller or medium-sized test systems. However, for the larger systems, such as, PNNL R3-12.47-2 feeder, the proposed method showcases significantly better results than the nonlinear centralized method; the nonlinear C-OPF problem failed to solve the loss minimization OPF problem (denoted as 'DNC*' - Did not converged) due to the scale of the OPF problem. On the contrary, both the nonlinear and approximated ENApp D-OPF method was able to solve the optimization problem with 5 communication rounds among neighboring area agents. The solutions are then verified by comparing the result with equivalent approximated C-OPF solution. This validates both the proposed approximated D-OPF and the proposed nonlinear D-OPF method, highlighting the advantage of the proposed distributed computation process.

Similarly, Table III validates the algorithm on the co-simulation platform for DER curtailment minimization problem for both the test systems. When no OPF is performed, there were voltage limit violation in the system. However, if operational limits are considered, the optimal generations are 5.166, 5.17, and 5.18 MW for approximated ENApp D-OPF, nonlinear ENApp D-OPF, and nonlinear C-OPF, respectively for the IEEE-123 bus test system. Similar to the loss minimization objective, the nonlinear C-OPF problem for the larger PNNL R3-12.47-2 feeder failed to solve; however, the proposed ENApp D-OPF method solved the DER curtailment minimization optimization problem (both approximated and the nonlinear problem) within 7 macro-iterations.

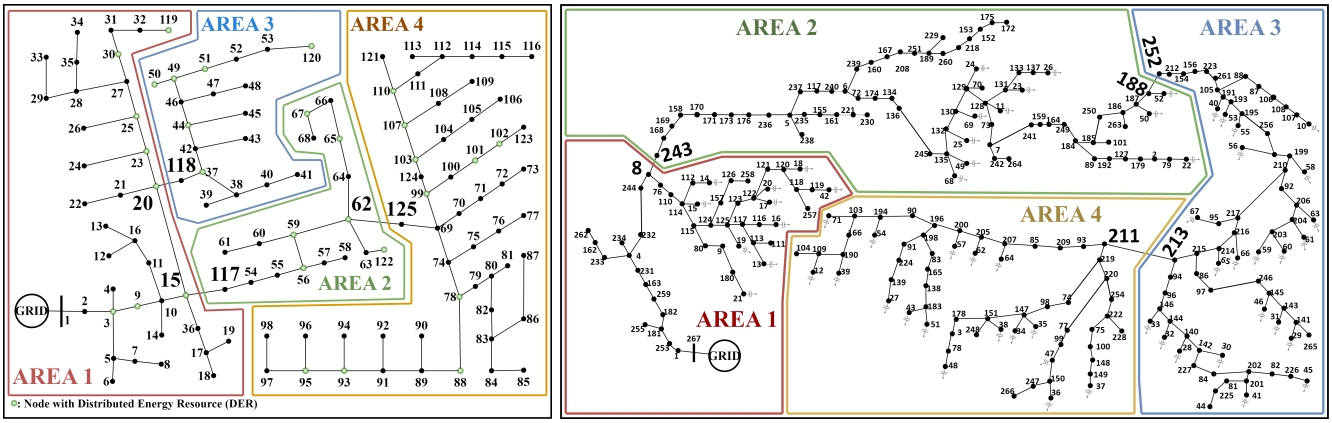

(a) Sectioned IEEE-123 Bus System

(b) Sectioned PNNL R3-12.47-2 feeder

Fig. 4. Simulated test systems to validate and compare the developed D-OPF algorithm

TABLE III. DER Curtailment Minimization Results Comparison

Method	Generation (MW)		Communication-round	
	IEEE-123 Bus System	PNNL R3-12.47-2 Feeder	IEEE-123 Bus System	PNNL R3-12.47-2 Feeder
Nonlinear Problem				
No OPF	5.400	7.642	-	-
C-OPF	5.180	DNC*	-	-
ENApp D-OPF	5.17	7.113	4	7
Approximated Problem				
C-OPF	5.102	7.065	-	-
ENApp D-OPF	5.166	6.946	6	4
ADMM D-OPF	5.140	7.642	6	54

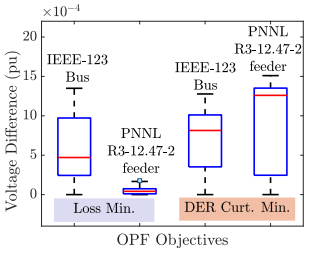

Fig. 5. Voltage Error

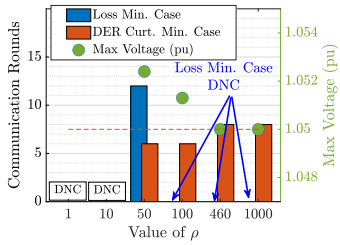

Fig. 6. ρ tuning for IEEE-123 bus

2) Feasibility: In addition to comparing the optimality of the solutions obtained from the proposed ENApp D-OPF methods, the feasibility of the solutions is also assessed. After implementing the optimal control decisions in a three-phase nonlinear power flow model (here using GridLAB-D), the derived node voltages are compared with the node voltage obtained from the OPF solution. Fig. 5 illustrates the distribution of the voltage differences between the approximated OPF solutions and the nonlinear power flow solutions upon applying the optimal control variables. For all the systems, and all the OPF objectives, the voltage differences are not higher than 10^{-3}, which translates to less than 0.15% difference in the node voltages. This demonstrates that all the power flow constraints have been satisfied, and thus validates the feasibility of the solution attained from the proposed ENApp D-OPF method.

C. Comparison with other methods

Besides providing the validation of the proposed D-OPF method, it is crucial to compare the results and convergence speed with other state-of-the-art D-OPF method. In this paper, the ADMM method has been compared with the proposed D-OPF method; approximated distributed problems have been solved to avoid convergence issues with ADMM algorithms. For the ADMM method, both the voltage and the complex power of the shared boundaries have been shared with both UA agent and DA agent. Specifically, in the implemented ADMM algorithm, each area solves the local problem and shares the solved variables for the shared nodes with the corresponding neighbor area. Those shared variables are real and reactive power and voltage. The two-norm difference between these shared boundary values is added to the objective function as in [4]. The penalty parameter ρ is set to be the same for all boundary values. Besides, generally the convergence of the ADMM method depends significantly on the tuning of the penalty parameter. The convergence of the nonlinear distributed problems are not guaranteed, and thus in this paper, the equivalent approximated (convex) problems are solved using the ADMM and the result is then compared with ENApp D-OPF method. Additionally, we have compared our method with state-of-the-art 3-phase feedback-based online D-OPF algorithm [26], [27].

1) Tuning of the ADMM: To ensure that the ADMM algorithm was fairly compared, each case was carefully tuned; the penalty parameters, ρ, are varied from 1 to 1000 for the OPF problems described above for both the test systems.

For the loss minimization OPF objective for the simulated IEEE-123 bus test system case, only ρ values of 40, 50, or 60, resulted in convergence. Fig. 6 demonstrates the convergence properties of the ADMM method for different ρ values. For this case different substation voltage, v_{sub}, values were also tested and ultimately $\rho = 50$ was chosen for further analysis since it had good performance and converged in all voltage cases. The substation voltage was chosen to be 1.05 p.u. for consistency with other cases. Similarly for the DER curtailment minimization OPF objective for the simulated IEEE-123 bus test system case, any value of ρ greater than about 40 was found to result in convergence. Values of $80 <= \rho <= 460$ resulted in the fastest convergence of six rounds, but ρ values lower than 200 yields voltage upper bound violation upon implementing the control variables in the nonlinear power flow solver of the model. Larger ρ values generally resulted in

This article has been accepted for publication in IEEE Transactions on Sustainable Energy. This is the author's version which has not been fully edited and content may change prior to final publication. Citation information: DOI 10.1109/TSTE.2024.3492976

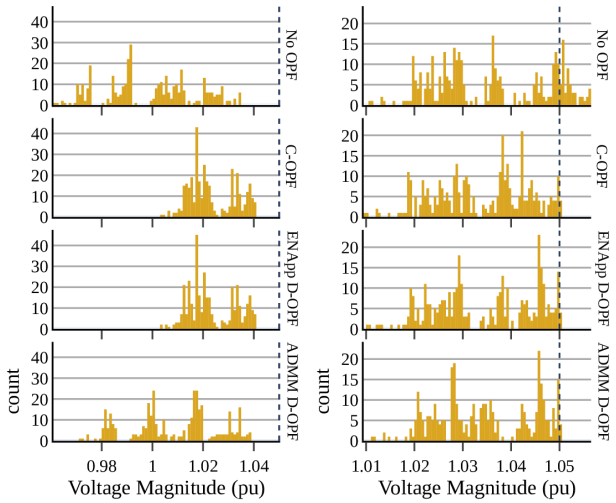

(a) Loss Minimization (b) DER Curtailment Minimization

Fig. 7. Voltage distribution for IEEE-123 bus test system.

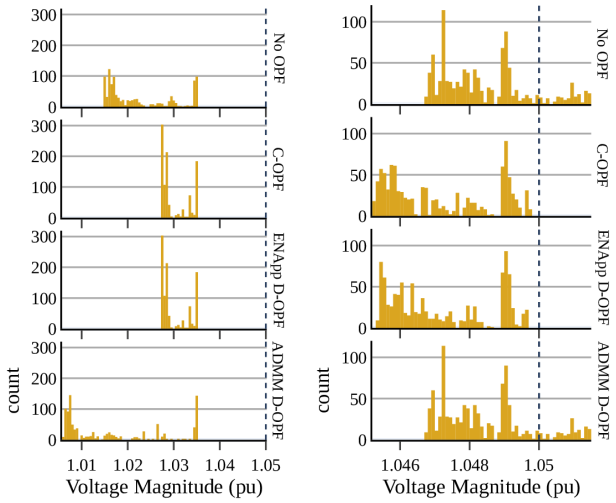

(a) Loss Minimization (b) DER Curtailment Minimization

Fig. 8. Voltage distributions for PNNL R3-12.47-2 feeder test system.

lower constraint violation but lower DER utilization as well. Ultimately $\rho = 460$ was chosen for further analyses since it only required 6 rounds and had no voltage violation (see Fig. 6). On the other hand, for the second (larger) test system, i.e., PNNL R3-12.47-2 feeder, the loss minimization OPF objective problem did not converge for any value of ρ for ADMM. However, for DER curtailment minimization OPF objective, ADMM converges for $\rho \geq 50$. Please note that, while the local sub-problems were solved successfully, the consensus was not attained at the boundaries of these sub-problems, leading to DNC condition.

2) Comparison with ADMM: While the state-of-the-art ADMM D-OPF has been tuned for the best performance of the algorithm, the process fails to converge to a meaningful solution for a medium/large-scale three-phase OPF problems. For the loss minimization OPF problem for the IEEE-123 bus test system, it took 12 macro-iterations to converge to a sub-optimal solution – objective value (line loss) is 38.954 kW compared to 26.546 kW of the ENApp D-OPF solution. For the large PNNL R3-12.47-2 feeder, ADMM failed to converge to any solution. For the DER curtailment minimization OPF objective, ADMM D-OPF converges to the solution after 6 macro-iterations for IEEE-123 bus test system, however fails to converge to a meaningful solution for the large PNNL R3-12.47-2 feeder after 54 macro-iterations. While this case does have boundary convergence after 54 rounds (table III), it does not actually reduce any DER output and therefore has no effect, and numerous voltage violations remain.

Briefly, given the best tuning for the ADMM algorithm for different objectives and test systems, the ADMM algorithm performs poorly compared to the proposed ENApp D-OPF method for medium systems, and fails completely for larger feeders. On the contrary, proposed ENApp D-OPF method solves both the approximated and the nonlinear distributed OPF problems for both the test systems.

In addition to the solution quality and speed of the process, the node voltage distribution of the whole system has been compared for both the ADMM method and the unbalanced ENApp D-OPF method. Specifically, the voltage distribution of the above mentioned two methods have been compared against the approximated C-OPF solution. Fig. 7 and 8 demonstrates the node voltage distribution of the overall network for different optimization methods. From Fig. 7, it is observed that for both the OPF objectives, the voltage distribution for the C-OPF and ENApp D-OPF is similar. However, for the ADMM method, only the DER curtailment minimization objective case has similar voltage distribution to the equivalent central problem; the voltage distribution for the loss minimization objective for IEEE-123 bus test system has more similarities to the case without any OPF than the C-OPF solution. Kindly refer to Table II for a comparison of the objective function values for different OPF methods. This trend can also be seen for the larger PNNL R3-12.47-2 feeder test case. Fig. 8 showcases the voltage distribution of the overall system for different optimization methods for PNNL R3-12.47-2 feeder. While ADMM method fails to solve for any OPF objectives, the voltage distribution from the ENApp D-OPF solution closely matches with the voltage distribution of the equivalent C-OPF solutions. On the contrary, ADMM fails to solve, and the voltage distribution for those cases remains similar to the case for "No OPF" scenarios. A comparison of the solution time for different OPF objectives for different D-OPF algorithm is reported in Table IV. Please note that the average time required to solve sub-problems is comparable for both methods, indicating that the proposed ENApp D-OPF method does not introduce additional complexity. However, ADMM requires a higher number of iterations, resulting in greater total computation time.

3) Comparison with Feedback-based Online Algorithm: The DER Curtailment Minimization problem with the IEEE-123 Bus test systems as described in Table I was run with a feedback-based D-OPF algorithm [26], [27]. The algorithm did not converge to an optimal solution after 1500 iterations. The max voltage of the system was 1.065 p.u., indicating a failure even after 1500 iterations.

This article has been accepted for publication in IEEE Transactions on Sustainable Energy. This is the author's version which has not been fully edited and content may change prior to final publication. Citation information: DOI 10.1109/TSTE.2024.3492976

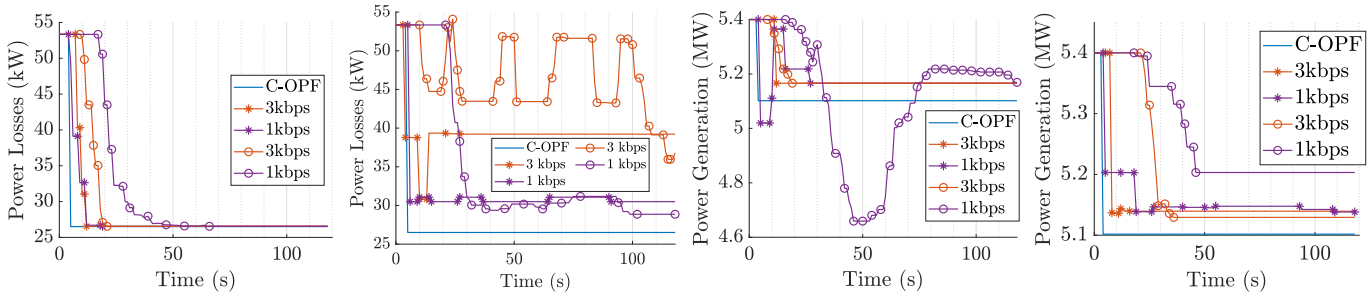

(a) ENApp D-OPF: Loss Min. (b) ADMM D-OPF: Loss Min. (c) ENApp D-OPF: DER Curt. Min. (d) ADMM D-OPF: DER Curt. Min.

Fig. 9. Communication stress test and the convergence of the D-OPF methods for IEEE-123 bus test system

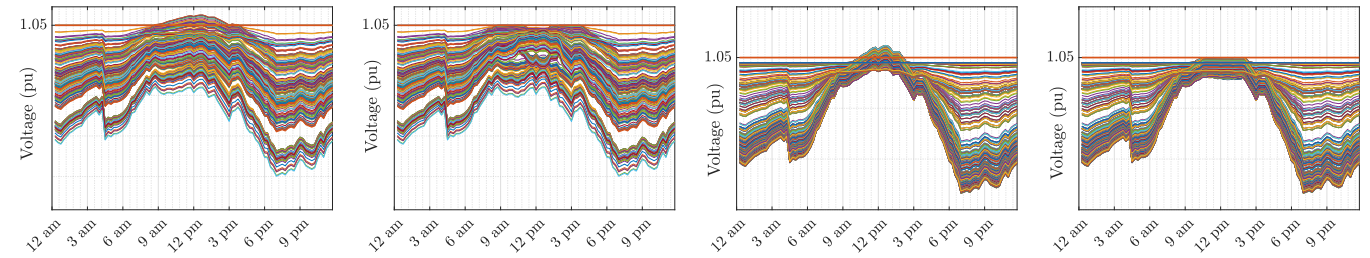

(a) IEEE-123 bus test system: without DER Curtailment Minimization OPF (b) IEEE-123 bus test system: with DER Curtailment Minimization OPF (c) PNNL R3-12.47-2 Feeder: without DER Curtailment Minimization OPF (d) PNNL R3-12.47-2 Feeder: with DER Curtailment Minimization OPF

Fig. 10. All the node voltages for a 24-hour time-series simulation: without and with OPF for DER curtailment minimization problem

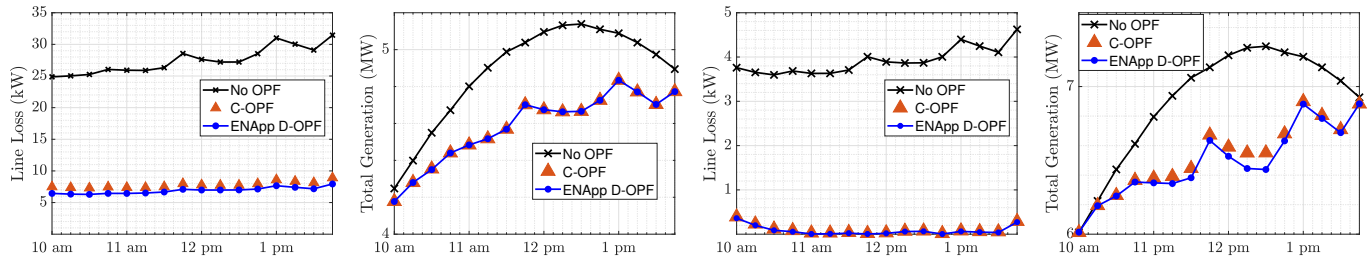

(a) IEEE-123 bus test system: Loss Minimization OPF. (b) IEEE-123 bus test system: DER Curtailment Minimization OPF (c) PNNL R3-12.47-2 Feeder: Loss Minimization OPF. (d) PNNL R3-12.47-2 Feeder: DER Curtailment Minimization OPF

Fig. 11. Comparison of objective values for different optimization problems for different distribution systems

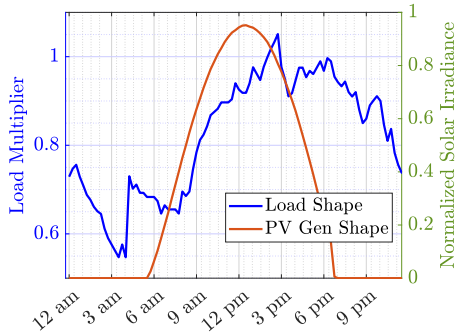

Fig. 12. Load shape and the PV irradiance for a 24-hour simulation

D. Effect of Communication

Next we test the robustness of the proposed algorithm, when subjected to poor communication network conditions; it is tested with two different communication network topologies (ideal and ring topology) for both the loss minimization problem and the DER curtailment minimization problem for medium IEEE-123 bus test system. In the ideal topology, each area controller has a direct link with its neighbors and with devices in its own area. In the ring topology all devices and controllers are connected in a single large loop without regard to physical location. Each link between network nodes is a point-to-point link with a negligible delay and has different bandwidths (3kbps, 2kbps, or 1kbps) to show the worst-case performance of the algorithm (see Fig. 9). The lines marked with circles indicate results run with the ring topology and lines marked with a star indicate the ideal topology. The blue line shows the results if no communication is allowed between controllers and the controllers have perfect communication links with local devices. There are several effects of poor communications that we have observed:

- If a controller doesn't receive data from either UA or DA

TABLE IV. Computational time comparison – Average solve time (s) per iteration for slowest area (approximated problems).

Method	DER Curtailment Minimization		Loss Minimization	
	IEEE-123 Bus System	PNNL R3-12.47-2 Feeder	IEEE-123 Bus System	PNNL R3-12.47-2 Feeder
ENApp D-OPF	0.31s	0.99s	0.48s	1.53s
ADMM D-OPF	0.29s	0.93s	0.44s	1.46s

because of data delays, it will falsely assume convergence and dispatch the inverters prematurely. When the delayed data does arrive it will continue iterating again.
- Delayed communication between areas does not prevent convergence except in extreme cases.
- The quality of the resulting solution as measured after convergence is not impacted by the communication delays.

E. Time-series Simulation

To showcase the practicality and efficiency of real-life implementation, as well as the comprehensiveness of the proposed method, a 24-hour simulation has been conducted using 15-minute resolution data for both the OPF objective (loss minimization and DER curtailment minimization) and for both the IEEE-123 bus test system and PNNL R3-12.47-2 feeder. Please note that while 15-minute resolution data is standard for solving active power distribution system related problems, the proposed method can solve OPF problems within minutes. Therefore, the proposed method is capable of addressing rapidly changing scenarios in distribution systems.

For the 24-hour simulation, same load shape and PV irradiance profile have been utilized to facilitate the replication of results (see Fig. 12). Fig. 10 illustrates the node voltages throughout the entire 24-hour simulation for DER curtailment minimization OPFs conducted on both IEEE-123 bus test system and PNNL R3-12.47-2 feeder. When no operational constraints are applied, i.e., no OPF is activated, around 10 am in the morning, the system voltage exceeds the ANSI limit of 1.05 p.u. for several nodes (Fig. 10(a), 10(c)). The over voltage persists in the system until 2 pm in the afternoon, as during this time window, the solar irradiance values are very high. This trend of over voltage scenarios are consistent for both the distribution systems. However, upon activation of the DER curtailment minimization OPF using the proposed ENApp D-OPF method, PV generations are minimally curtailed to ensure the distribution system operates within the ANSI limit for nodal voltages. Consequently, all node voltages in the system become bounded by the upper limit (Fig. 10(b), 10(d)).

Fig. 11 compares the objectives values for different OPF scenarios for both the distribution systems. Since the nonlinear solutions are not available for the large test systems, the approximated OPF problems have been solved, and upon enacting the optimal controls in the nonlinear power flow model, the objective values have been recorded. Also, the time window between 10 am and 2 pm yields more significant results for the optimization problems applied to the test systems throughout the day, thus the comparison of OPF objectives has been focused on that specific time window. For the loss minimization OPF problem, both the test systems attain significantly lower active power losses in the system compared to the base case where no OPF has been activated; further, the proposed ENApp D-OPF method obtain same objective values as the equivalent C-OPF method (Fig. 11(a), 11(c)). Similarly, DER curtailment minimization OPF problem illustrates similar results; the proposed ENApp D-OPF yields similar maximum total distributed power generations (or minimum active power curtailment) as the equivalent C-OPF solutions (Fig. 11(b), 11(d)), while maintaining the operation voltage limits (Fig. 10(b), 10(d)). These results demonstrates the real life applicability of the proposed ENApp D-OPF method for scaled unbalanced active power distribution systems.

F. Comprehensive System Model

In this section, we have extended the models for DERs within the optimal power flow (OPF) problem formulation to allow for both simultaneous real (P) and reactive (Q) power control. This enhancement broadens the applicability of our method by accommodating more complex and realistic operational scenarios where DERs can adjust both real and reactive power outputs concurrently to optimize system performance. Moreover, we incorporated voltage-dependent loads into the OPF formulation and added legacy device controls, such as regulator taps and capacitor bank (see Appendix). This integration improves the practicability of the OPF solution, and demonstrates the robustness to the complex OPF problems. The specific models are described below.

As a test system for the comprehensive system model, we have simulated the IEEE-123 bus system for loss minimization objective with voltage dependent loads, and legacy devices. Specifically, we have added regulators between Area 3 and Area 4 of the test system. The resulting MILP OPF problem were solved using SCIP solver. From the simulation results, it is observed that the D-OPF method converges within 54 seconds, and the total line losses in system is 28.75 kW. The equivalent centralized problem attains 28.51 kW of active power losses in the system which validates the optimality of the D-OPF solution. Additionally, upon implementing the D-OPF control variables in the nonlinear power flow model (OpenDSS), the maximum node voltage deviation between the linear model and the OpenDSS solution was 0.006 p.u., validating the feasibility of the D-OPF solution. This confirms that both the optimality and feasibility of the ENApp D-OPF problem, formulated with comprehensive system models, including legacy devices, simultaneous real and reactive power control, and voltage-dependent loads, have been thoroughly validated.

V. Conclusions

In this paper, a novel distributed optimal power flow method for radial three-phase, unbalanced power distribution system has been proposed. The proposed approach leverages the radial topology of the active distribution systems to improve the scalability and reduce overall solution speed. The proposed distributed coordination method for unbalanced power distribution systems achieves a converged network-level optimal solution using significantly fewer communication rounds for both nonlinear and the convex-approximated OPF problems. The performance of the proposed algorithm is evaluated using a cyber-power co-simulation environment with various communication network parameters, to validate the robustness of the proposed D-OPF algorithm under stressed communication. The proposed method is compared with traditional D-OPF methods and demonstrated higher quality of the solution when compared with equivalent central solutions. Additionally, the proposed method is able to solve nonlinear D-OPF problems within reasonable number of communication rounds for scaled PNNL R3-12.47-2 feeder system, where C-OPF problem fails

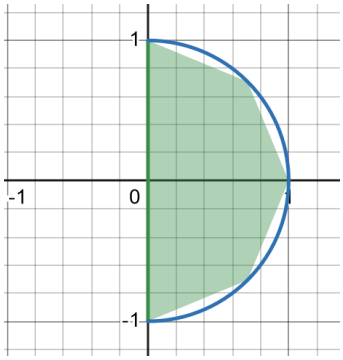

Fig. 13. Visualization of inverter linearization using inscribed polygon.

to converge to the solution. For various cases, it is shown that the proposed method successfully converges to the network-level optimal solution within reasonable time, even when the communication network is facing significant stress, such as, communication delays and a low bandwidth communication infrastructure. Furthermore, a 24-hour simulation case has been provided to so illustrate the efficacy of the proposed method for changing scenarios of the distribution system. In summary, The D-OPF algorithm is specifically tailored to meet the demands of these systems while also accounting for the critical role of communication networks in distributed control. Incorporating uncertainty in load profiles and other network data into the D-OPF framework is currently under consideration and is a part of our future work.

APPENDIX

This appendix summarizes the formulation of regulator tap settings, voltage-dependent load models, and simultaneous real and reactive power control models, that can be incorporated in the D-OPF formulation.

A. Regulator Taps

Let a_j^p be the turn ratio for the voltage regulator on phase p between node i and j. Let $u_{tap,k,j}^p \in 0, 1 \forall k \in \{1, 2, ..., 33\}$ be the binary variable for the regulator on phase p between node i and j; let $b_k \in \{0.9, 0.90625, ..., 1.1\}$. Then, the regulator can be modeled in the OPF formulation as equation (16).

$$B_k = b_k^2, A_j = a_i^2, V_j^p = a_j^p V_i^p, v_j^p = A_j^p v_i^p \tag{16a}$$

$$A_j^p = \sum_{k=1}^{33} B_k u_{tap,k,j}^p \tag{16b}$$

$$\sum_{k=1}^{33} u_{tap,k}^p = 1 \tag{16c}$$

B. Capacitor switch

Let $u_{cap,j}^p$ be the binary variable denoting the switch status of the capacitor bank at phase p of node j; then the capacitor can be modeled in the OPF formulation as equation (17).

$$q_{C,j}^p = u_{cap,j}^p q_{cap,j}^{rated,p} v_j^p \tag{17a}$$

C. Voltage dependent loads

Let CVR_p and CVR_q be the CVR factor that determines the voltage dependencies of real and reactive power loads, respectively; also, 0 subscript denotes the nominal load value at 1 p.u. voltage. Then the voltage dependent loads can be modeled in the OPF formulation as equation (18). For more details of CVR factors, please refer to [20].

$$p_{L,j}^p = p_{j,0}^p + \mathrm{CVR}_p \frac{p_{i,0}^p}{2}(v_j^p - 1) \tag{18a}$$

$$q_{L,j}^p = q_{j,0}^p + \mathrm{CVR}_q \frac{q_{i,0}^p}{2}(v_j^p - 1) \tag{18b}$$

D. Simultaneous P/Q control of DERs

The limits of active and reactive power injection of each DER can be described as a circle with radius $s_{D,j}^{rated}$ on the complex plane. It may also be limited to only produce active power and not absorb it, limiting its operation to the right half plane. To create linear limits we inscribe a polygon in the circle. In this instance we have used an octagon with vertices on the real and imaginary axis and at $\pm 45°$. This is described by (19) and illustrated by Fig. 13.

$$\sqrt{2}p_{D,j}^p + (\sqrt{2} - 2)q_{D,j}^p \leq \sqrt{2}s_{D,j}^{rated} \tag{19a}$$

$$\sqrt{2}p_{D,j}^p - (\sqrt{2} - 2)q_{D,j}^p \leq \sqrt{2}s_{D,j}^{rated} \tag{19b}$$

$$(-1 + \sqrt{2})p_{D,j}^p + q_{D,j}^p \leq s_{D,j}^{rated} \tag{19c}$$

$$(-1 + \sqrt{2})p_{D,j}^p - q_{D,j}^p \leq s_{D,j}^{rated} \tag{19d}$$

$$p_{D,j}^p \geq 0 \tag{19e}$$

REFERENCES

[1] H.-T. Yang and J.-T. Liao, "MF-APSO-based multiobjective optimization for PV system reactive power regulation," *IEEE Transactions on Sustainable Energy*, vol. 6, no. 4, pp. 1346–1355, 2015.

[2] M. Ross, C. Abbey, F. Bouffard, and G. Jos, "Multiobjective optimization dispatch for microgrids with a high penetration of renewable generation," *IEEE Transactions on Sustainable Energy*, vol. 6, no. 4, pp. 1306–1314, 2015.

[3] A. Castillo and R. P. O'Neill, "Survey of approaches to solving the ACOPF," *US Federal Energy Regulatory Commission, Tech. Rep*, 2013.

[4] D. K. Molzahn, F. Dörfler, H. Sandberg, S. H. Low, S. Chakrabarti, R. Baldick, and J. Lavaei, "A survey of distributed optimization and control algorithms for electric power systems," *IEEE Transactions on Smart Grid*, vol. 8, no. 6, pp. 2941–2962, 2017.

[5] J. D. Taft, P. De Martini, and R. Geiger, "Ultra-large-scale power system control and coordination architecture: A strategic framework for integrating advanced grid functionality," tech. rep., Pacific Northwest National Lab.(PNNL), Richland, WA (United States), 2014.

[6] S. Poudel, M. Mukherjee, R. Sadnan, and A. P. Reiman, "Fairness-aware distributed energy coordination for voltage regulation in power distribution systems," *IEEE Transactions on Sustainable Energy*, 2023.

[7] H. Qiu, W. Gu, and F. You, "Bilayer distributed optimization for robust microgrid dispatch with coupled individual-collective profits," *IEEE Transactions on Sustainable Energy*, vol. 12, no. 3, pp. 1525–1538, 2021.

[8] A. Rajaei, S. Fattaheian-Dehkordi, M. Fotuhi-Firuzabad, M. Moeini-Aghtaie, and M. Lehtonen, "Developing a distributed robust energy management framework for active distribution systems," *IEEE Transactions on Sustainable Energy*, vol. 12, no. 4, pp. 1891–1902, 2021.

[9] B. H. Kim and R. Baldick, "A comparison of distributed optimal power flow algorithms," *IEEE Transactions on Power Systems*, vol. 15, no. 2, pp. 599–604, 2000.

[10] W. Zheng, W. Wu, B. Zhang, H. Sun, and Y. Liu, "A fully distributed reactive power optimization and control method for active distribution networks," *IEEE Transactions on Smart Grid*, vol. 7, no. 2, pp. 1021–1033, 2015.

[11] S. Boyd, N. Parikh, E. Chu, B. Peleato, J. Eckstein, *et al.*, "Distributed optimization and statistical learning via the alternating direction method of multipliers," *Foundations and Trends® in Machine learning*, vol. 3, no. 1, pp. 1–122, 2011.

[12] X. Chang, Y. Xu, and H. Sun, "A distributed online learning approach for energy management with communication noises," *IEEE Transactions on Sustainable Energy*, vol. 13, no. 1, pp. 551–566, 2021.

[13] T. Erseghe, "Distributed optimal power flow using admm," *IEEE transactions on power systems*, vol. 29, no. 5, pp. 2370–2380, 2014.

[14] E. Dall'Anese, H. Zhu, and G. B. Giannakis, "Distributed optimal power flow for smart microgrids," *IEEE Transactions on Smart Grid*, vol. 4, no. 3, pp. 1464–1475, 2013.

[15] G. C. Kryonidis, K.-N. D. Malamaki, S. I. Gkavanoudis, K. O. Oureilidis, E. O. Kontis, J. M. Mauricio, J. M. Maza-Ortega, and C. S. Demoulias, "Distributed reactive power control scheme for the voltage regulation of unbalanced lv grids," *IEEE Transactions on Sustainable Energy*, vol. 12, no. 2, pp. 1301–1310, 2020.

[16] A. Bernstein and E. Dall'Anese, "Real-time feedback-based optimization of distribution grids: A unified approach," *IEEE Transactions on Control of Network Systems*, vol. 6, no. 3, pp. 1197–1209, 2019.

[17] S. Magnússon, G. Qu, and N. Li, "Distributed optimal voltage control with asynchronous and delayed communication," *IEEE Transactions on Smart Grid*, 2020.

[18] R. Sadnan and A. Dubey, "Distributed optimization using reduced network equivalents for radial power distribution systems," *IEEE Transactions on Power Systems*, vol. 36, no. 4, pp. 3645–3656, 2021.

[19] K. P. Schneider, B. Mather, Pal, *et al.*, "Analytic considerations and design basis for the IEEE distribution test feeders," *IEEE Transactions on power systems*, vol. 33, no. 3, pp. 3181–3188, 2017.

[20] R. R. Jha, A. Dubey, C.-C. Liu, and K. P. Schneider, "Bi-level volt-var optimization to coordinate smart inverters with voltage control devices," *IEEE Transactions on Power Systems*, vol. 34, no. 3, pp. 1801–1813, 2019.

[21] L. Gan and S. H. Low, "Convex relaxations and linear approximation for optimal power flow in multiphase radial networks," in *2014 Power Systems Computation Conference*, pp. 1–9, IEEE, 2014.

[22] B. Palmintier, D. Krishnamurthy, P. Top, S. Smith, J. Daily, and J. Fuller, "Design of the helics high-performance transmission-distribution-communication-market co-simulation framework," in *2017 Workshop on Modeling and Simulation of Cyber-Physical Energy Systems (MSCPES)*, pp. 1–6, IEEE, 2017.

[23] D. P. Chassin, K. P. Schneider, and C. Gerkensmeyer, "GridLAB-D: An open-source power systems modeling and simulation environment," in *IEEE/PES Transmission and Distribution Conference and Exposition*, pp. 1–5, IEEE, May 2008.

[24] NS-3 Network Simulator. https://www.nsnam.org/.

[25] K. P. Schneider, Y. Chen, D. P. Chassin, R. G. Pratt, D. W. Engel, and S. E. Thompson, "Modern grid initiative distribution taxonomy final report," tech. rep., Pacific Northwest National Lab.(PNNL), Richland, WA (United States), 2008.

[26] "OEDI-SI/scenarios/feedback-based d-OPF | open energy information."

[27] A. Bernstein and E. Dall'Anese, "Bi-level dynamic optimization with feedback," in *2017 IEEE Global Conference on Signal and Information Processing (GlobalSIP)*, pp. 553–557, 2017.

Rabayet Sadnan (Member, IEEE) received the B.Sc. and M.Sc. degrees in Electrical and Electronics Engineering from Bangladesh University of Engineering And Technology (BUET), Dhaka, Bangladesh, in 2015 and 2017, respectively. He also received M.Sc. in Mathematics in 2021 and Ph.D. in Electrical Engineering in 2023 from Washington State University (WSU), Pullman, WA, USA. Dr. Sadnan is currently appointed as power system research engineer at Pacific Northwest National Laboratory (PNNL). His research interests include sustainable energy, optimization, distribution system analysis, distributed optimization.

Nathan Gray (Student Member, IEEE) received a B.S. degree in electrical engineering from Walla Walla University and is working towards a Ph.D. in electrical power engineering at Washington State University. He is currently a research scientist at Pacific Northwest National Laboratory in Richland, WA, USA. His research interests include power distribution system resiliency and cyber-physical co-simulation.

Anjan Bose (Fellow, IEEE) Anjan Bose is a Regents Professor and the Distinguished Professor of Electric Power Engineering at Washington State University in Pullman, Washington. Dr. Bose is a Member of the US National Academy of Engineering and he is also a Fellow of the IEEE, a Fellow of the CSEE and a Distinguished Member of CIGRE. He was the recipient of the Outstanding Power Engineering Educator Award, the Third Millennium Medal, and the Herman Halperin Electric Transmission & Distribution Award from the IEEE. He is a leading researcher on the operation and control of the electric power grid. He has worked in the electric power industry as well as academe for over 50 years.

Anamika Dubey (Senior Member, IEEE) received the Ph.D. degree in electrical and computer engineering from The University of Texas at Austin, in December 2015. She is currently a Huie-Rogers Endowed Chair Associate Professor in electrical engineering with the School of EECS, Washington State University (WSU), Pullman. She also holds a joint appointment as a Research Scientist with the Pacific Northwest National Laboratory (PNNL). Her research interests include the optimization and control of large-scale electric power distribution systems for improved efficiency, flexibility, and resilience. Her expertise is in modeling, analyzing, and operating active power distribution systems with massive penetrations of controllable grid-edge resources (including DERs, EVs, and GEBs). She was a recipient of the National Science Foundation (NSF) CAREER Award.

Kevin P. Schneider (Fellow, IEEE) received his B.S. degree in Physics and his M.S. and Ph.D. degrees in Electrical Engineering from the University of Washington. His main areas of research are distribution system analysis and power system operations. He is currently a Laboratory Fellow at the Pacific Northwest National Laboratory, Manager of the Office of Electricity Sub-Sector, and a Research Professor at Washington State University as part of the PNNL/WSU Advanced Grid Institute (AGI). Dr. Schneider is an Affiliate Associate Professor at the University of Washington and a licensed Professional Engineer in Washington State. He is a Fellow of the Institute of Electrical and Electronic Engineers (IEEE), past chair of the Power Energy Society (PES) Distribution System Analysis (DSA) Sub-Committee, and the past Chair of the Analytic Methods for Power Systems (AMPS) Committee.